SAKARYA ÜNİVERSİTESİ
FEN BİLİMLERİ ENSTİTÜSÜ DERGİSİ

Sakarya University Journal of Science
SAUJS

ISSN 1301-4048 e-ISSN 2147-835X Period Bimonthly Founded 1997 Publisher Sakarya University
http://www.saujs.sakarya.edu.tr/

Title: Fluid-Structure Interaction Analysis of Carotid Artery Blood Flow with Machine Learning Algorithm and OpenFOAM

Authors: Murad KUCUR, Banu KÖRBAHTİ

Recieved: 2022-09-12 00:00:00

Accepted: 2022-10-08 00:00:00

Article Type: Research Article

Volume: 26
Issue: 6
Month: December
Year: 2022
Pages: 1131-1141

How to cite
Murad KUCUR, Banu KÖRBAHTİ; (2022), Fluid-Structure Interaction Analysis of Carotid Artery Blood Flow with Machine Learning Algorithm and OpenFOAM. Sakarya University Journal of Science, 26(6), 1131-1141, DOI: 10.16984/saufenbilder.1173983
Access link
https://dergipark.org.tr/en/pub/saufenbilder/issue/74051/1173983

Sakarya University Journal of Science 26(6), 1131-1141, 2022

Fluid-Structure Interaction Analysis of Carotid Artery Blood Flow with Machine Learning Algorithm and OpenFOAM

Murad KUCUR*[1], Banu KÖRBAHTİ[1]

Abstract

In this study, a patient-specific carotid artery model was analyzed with an open source program foam-extend. The research includes the effect of arterial wall deformation by fluid-structure analysis. Pulsatile velocity cycle is trained for 144 patients with different hemodynamic parameters, by machine learning algorithm using blood flow velocity measured from 337 points of the carotid artery. Data used for training is obtained from an open source in the literature. Here, the machine learning algorithm was created by the help of an open source code Phyton. Then, using trained values of machine learning, and the known systole and diastole blood pressures for a specific chosen patient, the patient-specific pulsatile velocity cycle was estimated. The estimated pulsatile velocity cycle was then fitted to Fourier series. This pulsatile velocity cycle is used as the input boundary condition for the model analyzed in foam-extend. The outlet boundary condition, pulsatile pressure cycle is found by 4-Element Windkessel algorithm. Wall shear stresses and time averaged wall shear stresses were obtained for both the rigid and fluid structure interaction models, and variation of displacement throughout the pulsatile cycle was found for the FSI model. Wall shear stresses, velocity, and displacements were obtained high at peak systole, consistent with pulsatile cycles. Like the wall shear stresses, the time averaged wall shear stresses for the FSI model were also found lower than the rigid model. The wall shear stresses showed an increase towards the exit of internal and external carotid artery.

Keywords: Open-FOAM, machine learning, carotid artery, blood flow

1. INTRODUCTION

Hemodynamic studies have an important place in the field of biomechanics. The changing behavior of blood flow, especially in narrowing and expanding vessels, poses an important problem for human health. In this emerging problem, it is vital to be able to predict the plaque formation and wall shear stresses that will occur as a result of the atherosclerosis, narrowing, and expansion of the vessels.

Machine learning methods are used in hemodynamics for prediction of wall shear

* Corresponding author: kucur@iuc.edu.tr
[1] Istanbul University-Cerrahpaşa, Engineering Faculty, Mechanical Engineering Department, Istanbul, Turkey.
E-mail: korbahti@iuc.edu.tr
ORCID: https://orcid.org/0000-0002-0356-0359, https://orcid.org/0000-0002-2579-5255

stresses, hypertension, pulsatile velocity, and pressure cycles. These investigations focus on carotid artery as well as aortic branches. Mostly, the prediction of pulsatile velocity and pressure cycles are made from the experimentally obtained Ultrasonic Doppler data [1, 2].

The researches conducted in the literature on carotid artery cover experimental and numerical works widely. The main aim in these investigations is determining the wall shear stresses (WSS), time averaged wall shear stresses (TWSS), oscillatory shear index (OSI), and relative residence time (RRT).

Many investigations have studied the effect of taking the flow as steady or pulsatile, and assuming the fluid is Newtonian or Non-Newtonian [3-6]. Among the various models available to study non-Newtonian flow, the Carreau-Yasuda, Power law, Carreau, and Casson models are mostly used. But the opinion is that, if the blood cells are small according to the vessel diameter, and blood vessel are large enough the fluid behaves like Newtonian [7]. The early studies considered the geometry of the carotid artery as 2-Dimensional [8], but after in the opinion of that the 3-Dimensional models can simulate the secondary flows in a better way, 3- Dimensional computer aided designed models are started to use. Nowadays, to take a realistic geometry, the researchers are using solid models based on patient-specific data of the carotid artery. The geometrical differences of the carotid artery also effect the flow characteristics. At that point, many investigations were carried out to see the effect of the bifurcation angle of the carotid artery and sinus region location. Because low shear stresses are responsible from the plaque formation, and these regions are the places where the low shear stresses occur.

Last years the investigations mostly focus on fluid-structure interactions (FSI) of the fluid and vessel wall. The studies showed that taking the vessel walls as rigid over-estimates the wall shear stresses slightly but this amount is still negligible. Lopes et al. [9] have carried out such research to show the difference between rigid and elastic wall approaches. They have concluded that rigid wall approach, overestimates the wall shear stresses, the higher elastic modulus produce lower displacement of the carotid artery walls. Lopes et al. [10] also have investigated the effect of the blood viscosity with FSI approach by taking the fluid as Newtonian and using Carreau-Yasuda viscosity model. They have found the WSS values higher, with Carreau-Yasuda model than, by taking the blood as Newtonian fluid. However, the displacement of the artery wall was not affected from the viscosity model. Wong et al. [11], have made FSI study with a geometry previously used by Tada et al. [12]. They have tried to establish a relationship between blood pressure, stenotic compression, and deformation. With their results, they have showed that a high level of compression and maximum WSS occurs in the stenotic apex and may be responsible from plaque formation. Kumar et al. [13], have carried out a 3-Dimensional FSI study using a patient carotid artery created by converting 2-Dimensional scan images from CT Angio data into a 3-Dimensional model using MIMICS. To better understand the formation and progression of atherosclerotic plaques in the carotid artery bifurcation, computer simulations were performed with different blood pressures, first normal and then indicative of hypertension. They have showed that the deformation of the artery, wall shear stress and especially oscillatory shear index highly affected from blood pressure variation. Lee et al. [14] also has performed 3-Dimensional FSI analysis with a carotid artery model reconstructed from patient specific clinical data. They have considered the effect of blood viscosity and have predicted the WSS values.

This research has focused on blood flow in the carotid artery, where stenosis and atherosclerosis are most commonly seen. The carotid artery model used here is patient-specific model that is taken from literature [15]. Computational Fluid Dynamics (CFD) analysis was done with foam-extend [16] (based on OpenFOAM) in order to get the wall shear stresses and displacement. Pulsatile velocity cycle as input boundary condition, and pulsatile pressure cycle as output boundary condition were obtained by machine learning algorithm and 4-Element Windkessel algorithm, respectively. The training data used in machine learning were taken from open source data in the literature [17, 18].

This study showed that using known systole and diastole blood pressures for a given patient, patient-specific pulsatile velocity cycle can be predicted with trained values of machine learning algorithm. In addition, the effect of the flexible structure of the vessel walls on the wall shear stresses was revealed by the fluid-structure interaction analysis on a patient-specific artery model.

2. PROBLEM FORMULATION AND METHODS

In this study, 3-Dimensional patient-specific solid model [15] of the arterial geometry was drawn from the dicom dataset by using VMTK program [19] and shown in Figure 1.

Carotid artery splits into two branches as internal carotid and external carotid artery. In this study, the diameter of the internal carotid artery (ICA) is 4.5 mm, and the diameter of external carotid artery (ECA) is 4.15 mm. The length and wall thickness of the artery is 81.6771 mm and 0.55 mm, respectively. The carotid artery was modelled as a linear elastic isotropic material and the mechanical properties of the vessel are taken as ρ_w = 1160 kg/m^3, v = 0.45, and E = 1.106 ×10^6 Pa. Here ρ_w is artery's wall density, v is Poisson ratio and E is elasticity modulus.

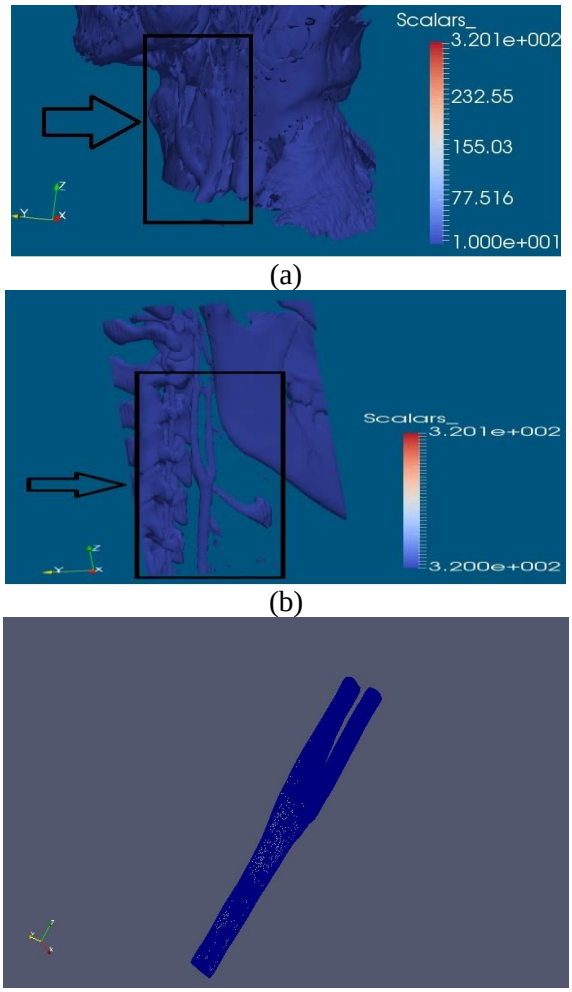

Figure 1 Carotid artery main geometry

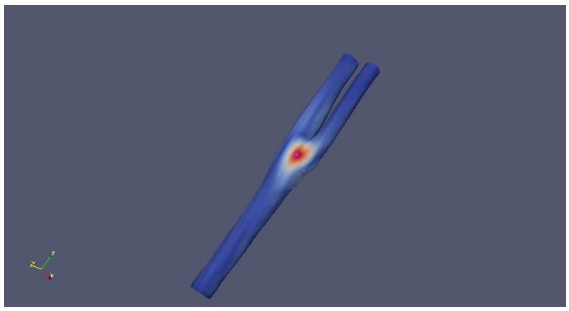
Figure 2 Mesh independency point

Mesh independency analysis was conducted for the displacement and velocity at the point shown at Figure 2 with tetrahedral elements ranging from 0.2 to 1 million, to determine the

accuracy of the solution. According to the results of the mesh independency study as shown in Figure 3, it was decided that the mesh structure constructed with 339872 elements for the solid domain and 934376 elements for fluid domain is sufficient.

Fluid structure interaction (FSI) simulations were made using the Foam-extend which is based on OpenFoam [16]. In simulations made with foam-extend, the solid model and the fluid model should fit together structurally. The absence of any gaps at the interfaces of the geometries is a necessary condition for simulation. The mesh structures of the geometries that interact correctly with each other structurally must also be compatible for simulation. For the fluid model with a higher mesh structure, the values after a certain mesh structure are also valid for the solid model.

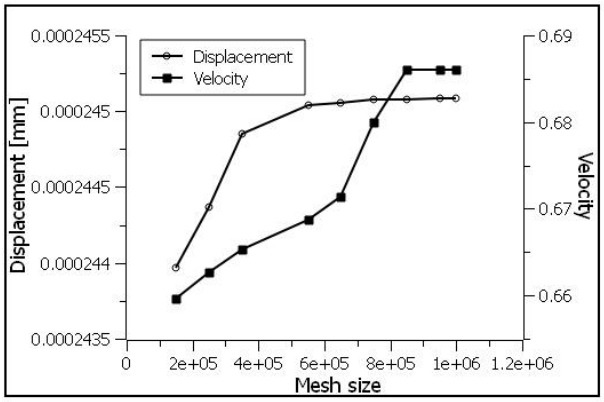

Figure 3 Mesh independency

Here, the blood flow in the carotid artery assumed as incompressible, laminar, and Newtonian. Blood density is taken as $\rho_f = 1060\ kg/m^3$ and the dynamic viscosity is $\mu = 3.71 \times 10^{-3} kg/m\ s$. The governing equations for the problem solved here are continuity and momentum equations.

Continuity equation is;

$$\nabla.\mathbf{u} = 0 \quad (1)$$

Momentum equation is;

$$\rho_f \left(\frac{\partial \mathbf{u}}{\partial t} + \mathbf{u}.\nabla\mathbf{u}\right) = -\nabla P + \mu\nabla^2\mathbf{u} \quad (2)$$

here **u,** P, and ρ_f is used as the velocity vector, static pressure, and fluid density, respectively. At the walls, the boundary conditions are no-slip so u=v=0.

The governing equation for artery wall deformation is the linear momentum equation expressed as [9,10],

$$\rho_s \left(\frac{\partial^2 w}{\partial t^2} - \vec{b}\right) - \nabla\sigma = 0 \quad (3)$$

Here, ρ_s is the structure density and w is the displacement of the arterial wall, b is body force and σ is the Cauchy stress tensor. Assuming linear isotropic structure, stress tensor can be represented as [9,10],

$$\sigma = 2\,\mu_L\varepsilon + \lambda_L tr(\varepsilon)I \quad (4)$$

μ_L and λ_L is the first and second Lame parameters respectively, ε is strain tensor, tr is trace function and I is identity matrix. Lame parameters are defined as functions of elasticity modulus and Poisson ratio [9,10].

$$\lambda_L = \frac{\upsilon E}{(1+\upsilon)(2\upsilon-1)} \quad (5)$$

$$\mu_L = \frac{E}{2(1+\upsilon)} \quad (6)$$

Wall shear stress is the frictional force per unit area applied by the blood on the surface of the arteries. In this study wall shear stresses are calculated as;

$$\vec{\tau}_w = \mu.(\omega_{wall}.\vec{n}) \quad (7)$$

here, ω_{wall} and $\vec{n}$ is the vorticity at the wall and the normal unit vector to the artery wall, respectively. Time averaged wall shear stresses (TWSS) during a pulsatile cycle are calculated as;

$$\mathrm{TWSS} = \frac{1}{\mathrm{T}} \int_0^{\mathrm{T}} |\overrightarrow{\tau_{\mathrm{w}}}| \ \mathrm{dt} \qquad (8)$$

where, T is the period of the pulsatile cycle.

The Support Vector Machine (SVC) [20] is an algorithm for learning effectively from a limited number of data. In this study, 144 patient's data from a small number of data sets were processed using the Support Vector Machine algorithm from the data file downloaded from the relevant web page [17, 18]. Systolic blood pressure, SBP; Diastolic blood pressure, DBP; Mean blood pressure, MBP; stroke volume, SV; and cardiac output, CO were taken as the hemodynamic properties of these patients. Pulsatile velocity cycle was trained by taking 337 velocity points for each 144 patients from the open source literature [17, 18]. Using the machine learning algorithm, 337 velocity points were taught depending on these five hemodynamic parameters that differ according to each patient. First of all, the accuracy of the machine learning result was checked by considering the 14th patient in the existing file. Here, the score of the learning algorithm (accuracy score) was obtained as 1. The rbf kernel function is used in the SVC algorithm.

Table 1 Hemodynamic specifications of 14th patient [17, 18]

SV [ml]	66.277
CO [L/min]	4.826
SBP [mmHg]	117.12
DBP [mmHg]	70.823
MBP [mmHg]	86.257
HR [bpm]	75
Tcardiac [s]	0.8

Table 1 shows the hemodynamic parameters for 14th patient. According to these parameters, by machine learning algorithm pulsatile velocity cycle is obtained for 14th patient and was compared with the original cycle that can be obtained from the open access data set [17, 18] and shown in Figure 4.

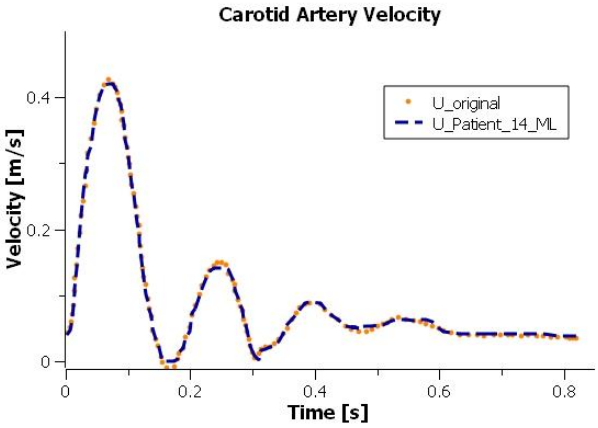

Figure 4 Velocity estimation results for 14th patient

Figure 4 shows a very good agreement between the original values and the predicted values for 14th patient.

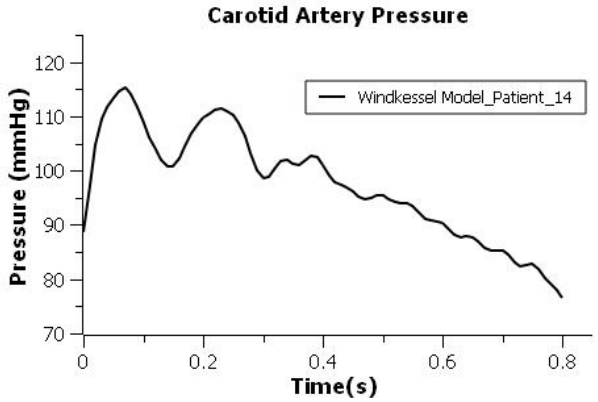

Figure 5 Pulsatile pressure cycle for 14th patient

Pressure pulse cycle is obtained by using 4-Element Windkessel model and shown in Figure 5.

After these validations for the learning result, the hemodynamic parameter values were determined for a completely different selected patient, and the velocity profile that would emerge for this patient with the previous learning was obtained. The hemodynamic values of this specially selected patient are given in Table 2, and the pulsatile velocity and

pulsatile pressure cycles are shown in Figure 6 and Figure 7, respectively.

Table 2 Hemodynamic values of a patient

SV [ml]	62
CO [L/min]	4.5
SBP [mmHg]	120
DBP [mmHg]	75
MBP [mmHg]	90
HR [bpm}	75
Tcardiac [s]	0.8

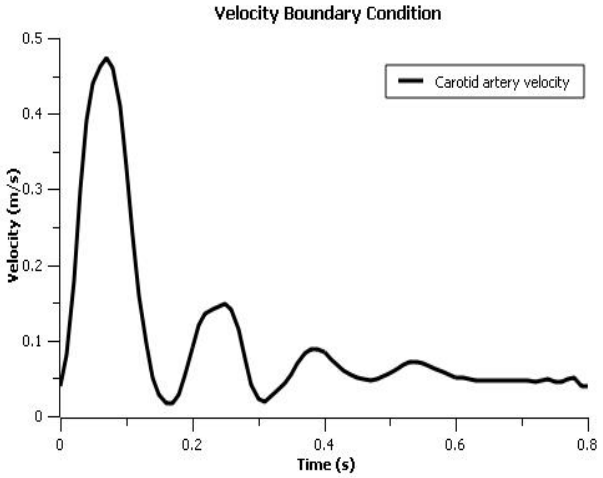

Figure 6 The pulsatile velocity cycle

The pulsatile velocity cycle in Figure 6 was used as inlet boundary condition for CFD analysis.

Also, the pulsatile velocity and pressure cycles are expressed as Fourier series in Equation 9 and 10, respectively. The coefficients of the series are given in Table 3. The frequency, ω for both equations is 7.85398.

$$V = a_0 + \sum_{n=1}^{20} a_n cosn\omega t + \sum_{n=1}^{20} b_n sinn\omega t \quad (9)$$

$$P = a_0 + \sum_{n=1}^{15} a_n cosn\omega t + \sum_{n=1}^{15} b_n sinn\omega t \quad (10)$$

Table 3 Parameters for pulsatile velocity and pressure cycles

Coefficients	Velocity cycle	Pressure cycle
a_0	0.101388	96.78016
a_1	0.058847	-2.12215
a_2	0.027928	-0.87664
a_3	0.00765	0.48207
a_4	-0.02192	0.706841
a_5	-0.06202	-1.46143
a_6	-0.02518	-2.42601
a_7	-0.01349	-1.08502
a_8	-0.01019	-1.20661
a_9	-0.00288	-0.76442
a_{10}	-0.00355	-0.28466
a_{11}	-0.0045	-0.36057
a_{12}	-0.00209	-0.36565
a_{13}	-0.00506	-0.05564
a_{14}	-0.00418	-0.96011
a_{15}	-0.00033	-0.82192
a_{16}	-0.00126	-
a_{17}	-0.00094	-
a_{18}	0.000103	-
a_{19}	0.000225	-
a_{20}	0.000125	-
b_1	0.051645	11.5202
b_2	0.062584	4.754548
b_3	0.060867	3.21535
b_4	0.059719	3.637598
b_5	0.02457	4.601801
b_6	-0.0153	1.281552
b_7	-0.00544	1.00616
b_8	-0.00743	0.870868
b_9	-0.00482	0.165459
b_{10}	-0.00141	0.43652
b_{11}	-0.00184	0.663278
b_{12}	-0.00154	0.31772
b_{13}	-0.00024	0.86716
b_{14}	-0.00453	0.823721
b_{15}	-0.00344	-0.06602
b_{16}	-0.00159	-
b_{17}	-0.00242	-
b_{18}	-0.00211	-
b_{19}	-0.00108	-
b_{20}	-2.6E-05	-

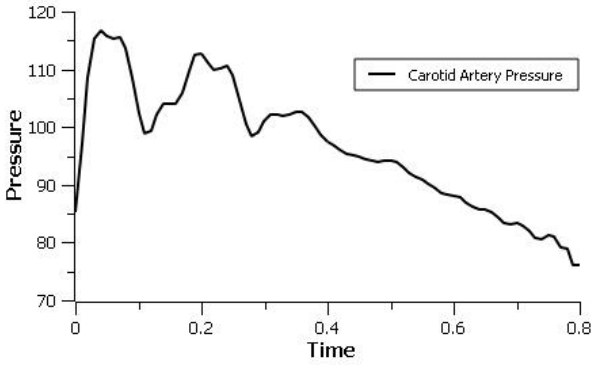

Figure 7 The pulsatile pressure cycle

3. RESULTS AND DISCUSSION

In the fluid-structure interaction analysis performed in this study, the displacements and the wall shear stresses were acquired throughout the pulsatile cycle. Wall shear stresses were obtained both for rigid and FSI model, and then compared at the peak of systole, and diastole.

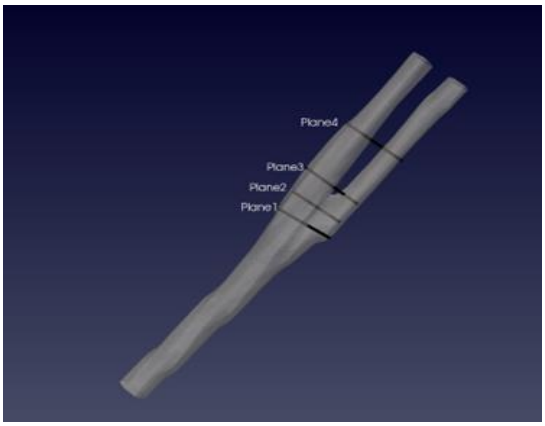

Figure 8 The planes for wall shear stresses

Figure 8 shows the planes where the wall shear stresses are obtained.

Average wall shear stresses throughout the pulsatile cycle for rigid and FSI models are shown in Figure 9 and Figure 10, respectively. WSS are slightly higher in rigid model than FSI. In both cases, at all planes the maximum WSS appears at systolic peak. WSS during systolic peak and diastole increases towards outlet of ICA and ECA. Table 4 gives this comparison. The WSS variation shows similar trend for both cases.

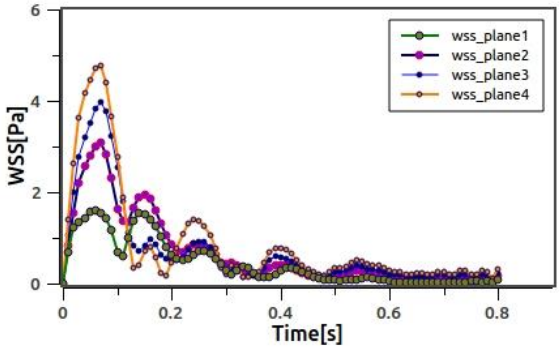

Figure 9 Wall shear stresses variation for rigid model

Table 4 Comparison of wall shear stresses for FSI and rigid model at systolic peak, and diastole

	Systolic Peak		Diastole	
	FSI model WSS [Pa]	Rigid model WSS [Pa]	FSI model WSS [Pa]	Rigid model WSS [Pa]
Plane 1	1.298	1.532	0.0551	0.0872
Plane 2	2.599	3.072	0.1911	0.2183
Plane 3	3.585	3.975	0.2190	0.2977
Plane 4	4.097	4.769	0.3429	0.3895

Figure 11 and 12 represents the time averaged wall shear stresses for FSI and rigid models, respectively. For both cases TWSS is high at the bifurcation point because of separation of flow at that point, velocity gradients are high so due to this TWSS is high at that region.

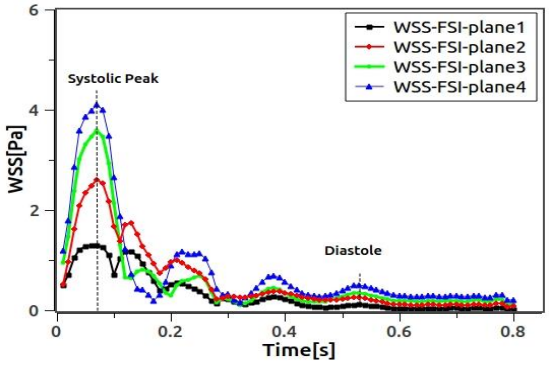

Figure 10 Wall shear stresses variation for FSI model

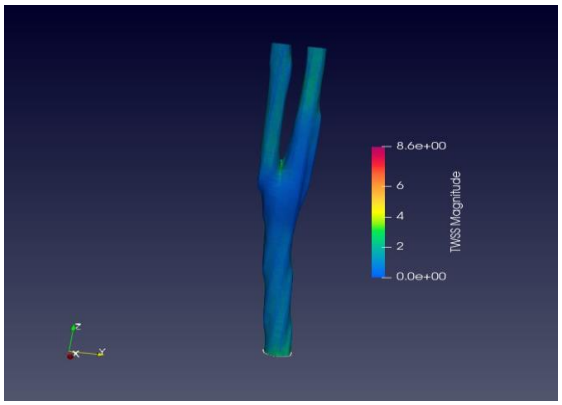

Figure 11 TWSS variation for FSI model

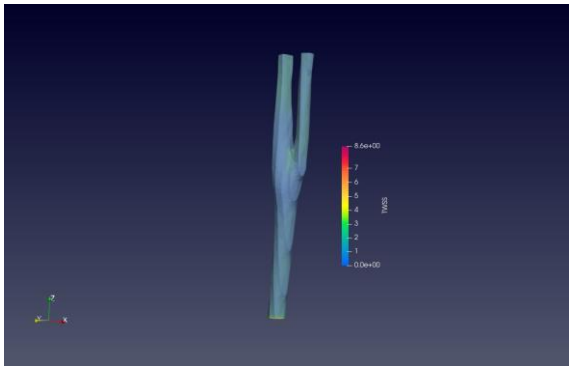

Figure 12 TWSS variation for rigid model

Table 5 shows a comparison of TWSS values between rigid and FSI models. Like the WSS values, TWSS values for the FSI model are lower than for the rigid model, and TWSS also increases towards the outlet of ICA and ECA.

Table 5 Comparison of time averaged wall shear stresses for FSI and rigid model

	FSI model TWSS [Pa]	Rigid model TWSS [Pa]
Plane 1	0.11665	0.32298
Plane 2	0.12188	0.36912
Plane 3	0.16003	0.46383
Plane 4	0.66452	0.77702

Figure 14 gives the variation of velocity at the location shown in Figure 13, Figure 16 gives the variation of WSS at the location shown in Figure 15 for both rigid and FSI models.

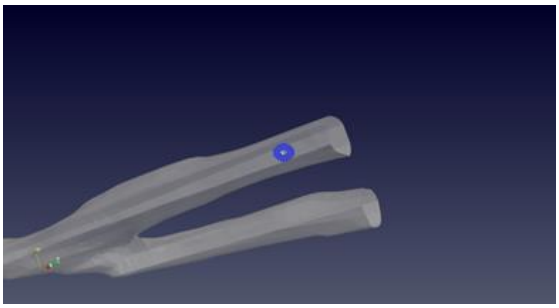

Figure 13 The location of velocity point

Wall shear stresses take their highest values during the pulsatile cycle near the peak of systole. Subsequently, after the peak of systole the wall shear stresses tend to decrease. Like WSS, velocity is also higher throughout all the pulsatile cycle for rigid model.

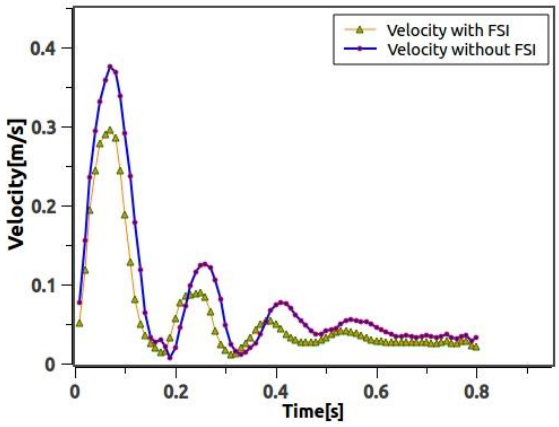

Figure 14 Variation of velocity for rigid and FSI models

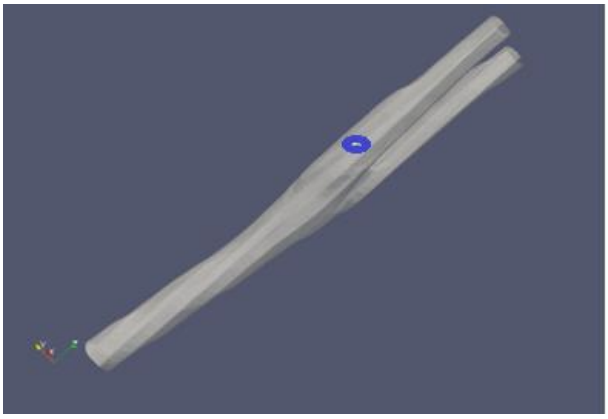

Figure 15 The location of wall shear stress point

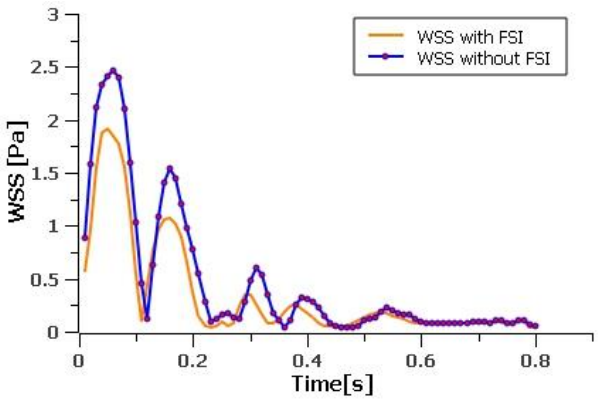

Figure 16 Variation of WSS for rigid and FSI models

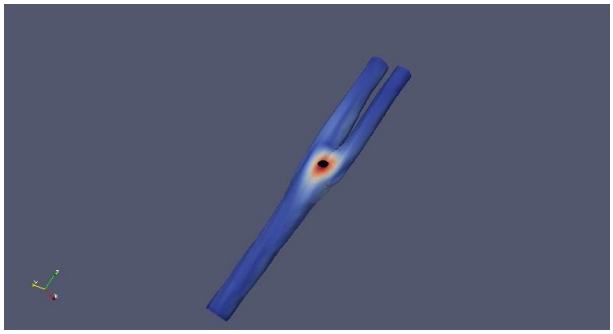

Figure 17 The location of displacement point

Figure 18 gives the variation of displacement at the location shown in Figure 17 for FSI model. The displacement decreases during the pulsatile cycle, maximum displacement appears at systolic peak. This is consistent with the pressure cycle, pressure is also high at systolic peak.

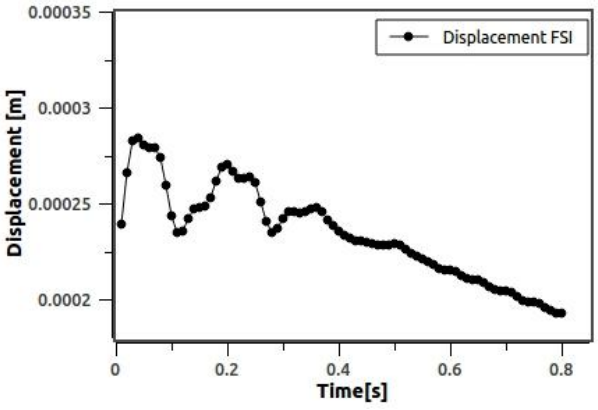

Figure 18 Variation of displacement

4. CONCLUSION

Areas of low wall shear stresses are responsible for the formation of atherosclerosis. In this study, the variation of wall shear stresses and displacements during the pulsatile cycle were investigated by considering the fluid structure interaction. Here, the input boundary condition, the pulsatile velocity cycle, was obtained for an independent patient by teaching the data from the literature with machine learning method.

In accordance with the studies in the literature, in this study, the rigid model revealed higher wall shear stresses than the FSI model. Wall shear stresses along the branches of the carotid artery decrease in both the rigid and FSI models. Wall shear stresses, velocity, and displacements are highest at the peak of systole consistent with the pulsatile cycles.

Funding
The author (s) has no received any financial support for the research, authorship, or publication of this study.

Authors' Contribution
The authors contributed equally to the study.

The Declaration of Conflict of Interest/ Common Interest
No conflict of interest or common interest has been declared by the authors.

The Declaration of Ethics Committee Approval
This study does not require ethics committee permission or any special permission.

The Declaration of Research and Publication Ethics
The authors of the paper declare that they comply with the scientific, ethical and quotation rules of SAUJS in all processes of the paper and that they do not make any falsification on the data collected. In addition,

they declare that Sakarya University Journal of Science and its editorial board have no responsibility for any ethical violations that may be encountered, and that this study has not been evaluated in any academic publication environment other than Sakarya University Journal of Science.

REFERENCES

[1] P. Çeltikçi, Ö. Eraslan, M. A. Atıcı, I. Conkbayır, O. Ergun, H. Durmaz, E. Çeltikçi, "Application of machine learning algorithms for predicting internal carotid stenosis and comparing their value to duplex Doppler ultrasonography criteria," Pamukkale Medical Journal, vol. 15, no. 2, pp. 213-222, 2022.

[2] S. Savaş, N. Topaloğlu, Ö. Kazcı, P. N. Koşar, "Comparison of deep learning models in carotid artery Intima-Media thickness ultrasound images: CAIMTUSNet," Bilişim Teknolojileri Dergisi, vol. 15, no. 1, pp. 1-11, 2022.

[3] K. Perklot, M. Resch, H. Florian, "Pulsatile Non-Newtonian flow characteristics in a three-dimensional human carotid bifurcation model," Journal of Biomechanical Engineering, Transactions of the ASME, vol. 113, pp. 464-475, 1991.

[4] F. Yubo, J. Wentao, Z. Yuanwen, L Jinchuan, C. Junkai, D. Xiaoyan, "Numerical Simulation of Pulsatile Non-Newtonian Flow in the Carotid Artery Bifurcation," Acta Mechanica Sinica, vol. 25, no. 249, pp. 249-255, 2009.

[5] J. Moradicheghamahi, J. Sadeghiseraji, M. Jahangiri, "Numerical solution of the pulsatile, Non-Newtonian and turbulent flow in a patient specific elastic carotid artery," International Journal of Mechanical Sciences, vol. 150, pp. 393-403, 2019.

[6] N. Kumar, S. M. Abdul Khader, R. B. Pai, P. Kyriacou, S. Khan, K. Prakashini, R. Srikanth, "Effect of Newtonian and Non-Newtonian flow in subject specific carotid artery," Journal of Engineering Science and Technology, vol. 14, no. 4, pp.2746-2763, 2020.

[7] D. N. Ku, "Blood flow in arteries," Annual Review of Fluid Mechanics, vol. 29, pp. 399-434, 1997.

[8] B. K. Bharadvaj, R. F. Mabon, D. P. Giddens, "Steady flow in a model of the human carotid bifurcation part I- flow visualization," Journal of Biomechanics, vol. 15, pp. 349-362, 1982.

[9] D. Lopes, H. Puga, J. C. Teixeira, S. F. Teixeria, "Influence of arterial mechanical properties on carotid blood flow: comparison of CFD and FSI studies," International Journal of Mechanical Sciences, vol. 160, pp. 209-218, 2019.

[10] D. Lopes, H. Puga, J. C. Teixeira, S. F. Teixeria, "Fluid-Structure interaction study of carotid blood flow: Comparison between viscosity models," European Journal of Mechanics/ B Fluids, vol. 83, pp. 226-234, 2020.

[11] K. K. L. Wong, P. Thavornpattanapong, S. C. P. Cheung, J. Y. Tu, "Biomechanical investigation of pulsatile flow in a three-dimensional atherosclerotic carotid bifurcation model," Journal of Mechanics in Medicine and Biology, vol. 13, pp.1-21, 2013.

[12] S. Tada, M. Tarbell, “A Computational study flow in a compliant carotid bifurcation-stress phase angle correlation with shear stress,” Annals of Biomedical Engineering, vol. 33, no. 9, pp.1202-1212, 2005.

[13] N. Kumar, S. M. Abdul Khader, R. Pai, S. H. Khan, P. A. Kyriacou, “Fluid structure interaction study of stenosed carotid artery considering the effects of blood pressure,” International Journal of Engineering Science, vol. 154, pp.1-14, 2020.

[14] S. H. Lee, S. Kang, N. Hur., S. Jeong, “A Fluid-Structure interaction analysis on hemodynamics in carotid artery based on patient specific clinical data,” Journal of Mechanical Science and Technology, vol. 26, pp. 3821-3831, 2012.

[15] Dr. M. Itagaki. (2019, September.30). The Biomedical 3D Printing Community, Available : http://www.embodi3d.com/ files /file/8523-head-and-neck-ct-dicom-dataset-for-teaching/.

[16] B. Gschaider, H. Rusche, H. Jasak, H. Nilsson, M. Beaudoin, V. Skuric. (2013, December.30). Sourceforge, Available : http: //sourceforge.net/p/foamextend/wiki/Home.

[17] P. H. Charlton, M. H. Jorge, V. Samuel, L. Ye, A.Jordi. (2019, April.10). Available : http://doi.org/10.528 /zenodo.3275625

[18] P. H. Charlton, M. H. Jorge, V. Samuel, L. Ye, A. Jordi, “Modelling arterial pulse waves in healthy aging: a database for in silico evaluation of hemodynamics and pulse wave indexes,” American Journal of Physiology-Heart and Circulatory Physiology, vol. 317, no. 5, pp. 1062-1085, 2019.

[19] [19] L. Antiga, D. Steinman, S. Manini, R. Izzo. (2018, March.20). Vascular Modeling Toolkit, Available : http://www.vmtk.org.

[20] [20] C. Cortes, V. Vapnik, "Support-vector networks," Machine Learning, vol. 20, pp. 273-297, 1995.